show "turnover", though showing a tendency of saturation in the region of our experiments. It is difficult to find stronger quenchers that form a stable monolayer without a large change in LB molecular assembly.

In conclusion, the emission of the excited carbazole chromophore in DDA/Cz polymer monolayers was quenched effectively by a small amount of the pyridinium quenchers placed in a directly contacting monolayer with the involvement of energy migration between the Cz chromophores. The quenching efficiency was varied by the mole fraction of carbazole contents, which is related to the density of excimer sites in the monolayer and to the redox potentials of the pyridiniums. It can be said that the efficiency of quenching in the copolymer monolayer is determined by the result of the competition of energy migration between the energy-trapping site (excimer formation site) and the carbazole chromophore just facing to the pyridinium quencher.

Acknowledgment. We thank Professor T. Yotsuyanagi, Tohoku University, for his kind support. This work was partly supported by a Grant-in-Aid for Scientific Research (No. 03403015) from the Ministry of Education, Science, and Culture of Japan.

References and Notes

(1) Polymer Langmuir–Blodgett Films Containing Photofunctional Groups. 5.[1] Part 1: Miyashita, T.; Yatsue, T.; Mizuta, Y.; Matsuda, M. *Thin Solid Films* **1990**, *179*, 439. Part 2: Miyashita, T.; Yatsue, T.; Matsuda, M. *J. Phys. Chem.* **1991**, *95*, 2448. Part 3: Mizuta, Y.; Matsuda, M.; Miyashita, T. *Macromolecules* **1991**, *24*, 5459. Part 4: Miyashita, T.; Matsuda, M.; Van der Auweraer, M.; De Schryver, F. C. Unpublished results.
(2) *Photoinduced Electron Transfer*; Fox, M. A., Chanon, M., Eds.; Elsevier: Amsterdam 1988; Parts A–D.
(3) Kuhn, H. *Phys. Rev.* **1986**, *A34*, 3409.
(4) Calvin, M. *Photochem. Photobiol.* **1976**, *23*, 425.
(5) Möbius, M. *Mol. Cryst. Liq. Cryst.* **1983**, *96*, 319.
(6) Miyashita, M.; Murakata, T.; Yamaguchi, Y.; Matsuda, M. *J. Phys. Chem.* **1985**, *89*, 497.
(7) Fendler, J. H. *J. Phys. Chem.* **1985**, *89*, 2730.
(8) Penfield, K. W.; Miller, J. R.; Paddon-Row, M. N.; Cotsairs, E.; Oliver, A. M.; Hush, N. S. *J. Am. Chem. Soc.* **1987**, *109*, 5061.
(9) Deronzier, A.; Essakalli, M. *J. Phys. Chem.* **1991**, *95*, 1737.
(10) Blodgett, K. B.; Langmuir, I. *Phys. Rev.* **1937**, *51*, 964.
(11) Kuhn, H.; Möbius, D.; Bücher, H. *Physical Methods of Chemistry*; Weisserberger, A., Rossiter, B. W., Eds.; Wiley: New York, 1972; Vol. 1, Part 3B, p 577.
(12) Gaines, G. L., Jr. *Insoluble Monolayers at Liquid–Gas Interface*; Wiley-Interscience: New York, 1966.
(13) Su, W. F. A.; Kurata, T.; Nobutoki, H.; Koezuka, H. *Langmuir* **1992**, *8*, 915.
(14) Ahuja, R. C.; Matsumoto, M.; Möbius, D. *J. Phys. Chem.* **1992**, *96*, 1855.
(15) Tamai, N.; Yamazaki, T.; Yamazaki, I. *J. Phys. Chem.* **1987**, *91*, 841.
(16) Yamazaki, I.; Tamai, N.; Yamazaki, T.; Murakami, A.; Mimuro, M.; Fujita, Y. *J. Phys. Chem.* **1988**, *92*, 5035.
(17) Miyashita, T.; Yoshida, H.; Murakata, T.; Matsuda, M. *Polymer* **1987**, *28*, 311.
(18) Miyashita, T.; Yoshida, H.; Itoh, H.; Matsuda, M. *Nippon Kagaku Kaishi* **1987**, 2169.
(19) Miyashita, T.; Mizuta, Y.; Matsuda, M. *Br. Polym. J.* **1990**, *22*, 327.
(20) See ref 1, part 2.
(21) Mort, P. J. *J. Non/Cryst. Solids* **1870**, *4*, 132.
(22) Okamoto, K.; Itaya, A.; Kusabayashi, S. *Polym. J.* **1975**, *7*, 622.
(23) Mort, J.; Chen, I.; Emerland, R. L.; Sharp, J. H. *J. Appl. Phys.* **1972**, *432*, 2285.
(24) Yokoyama, M.; Hanabata, M.; Tamamura, T.; Nakano, T.; Mikawa, H. *J. Chem. Phys.* **1977**, *67*, 1742.
(25) Kim, N.; Stephen, E. W. *Macromolecules* **1985**, *18*, 741.
(26) Mann, C. K.; Barnes, K. K. *Electrochemical Reactions in Nonaqueous System*; Marcel Dekker: New York, 1970.
(27) Murov, S. L. *Handbook of Photochemistry*; Marcel Dekker: New York, 1973.
(28) Brelman, I. B. *Energy Transfer of Aromatic Compounds*; Academic: New York, 1973.
(29) Seefeld, K.-P.; Möbius, D.; Kuhn, H. *Helv. Chim. Acta* **1977**, *60*, 2608.
(30) McLendon, G. *Acc. Chem. Res.* **1988**, *21*, 160.
(31) Miller, J. R.; Beitz, J. V. *J. Chem. Phys.* **1981**, *74*, 6746.
(32) Beitz, J. V.; Miller, J. R. *J. Chem. Phys.* **1979**, *71*, 4579.
(33) Marcus, R. A. *J. Chem. Phys.* **1956**, *24*, 966.
(34) Miller, J. R.; Beitz, J. V.; Huddleston, R. K. *J. Am. Chem. Soc.* **1984**, *106*, 5057.

Multiphoton Excitation, Dissociation, and Ionization of C_{60}

Peter Wurz and Keith R. Lykke*

Materials Science/Chemistry Divisions, Argonne National Laboratory, 9700 S. Cass Avenue, Argonne, Illinois 60439 *(Received: July 30, 1992)*

We show that the interaction of intense laser light in the visible and UV wavelength range with gas-phase C_{60} leads to high internal excitation of the parent molecule, rather than direct multiphoton ionization. High internal energies (≈50 eV) are achieved by absorption of 10–20 photons and rapid conversion from electronic to vibrational excitation. Thus, direct ionization of C_{60} by multiphoton absorption is in strong competition with other processes, mainly delayed ionization and fragmentation. A wide fluence and wavelength range is investigated to map out the different parameters that characterize these processes. Both delayed ionization and fragmentation have these high internal excitations as common precursors. These processes are successfully modeled by quasi-equilibrium theory. The results of this study indicate for the first time that the majority of ionization for fullerenes results from thermionic electron emission, a process that takes place on the time scale of microseconds.

Introduction

The first observation of high-mass carbon molecules[1] and the following discovery of the special stability of one of them, namely, C_{60},[2] started a new and exciting field of research. In particular, the disclosure of a simple and straightforward method to synthesize and isolate macroscopic quantities of these molecules[3] stimulated many laboratories to establish research programs on C_{60} and other fullerenes. Many experiments have already been performed, and some practical uses for C_{60} have also been postulated.[4,5] Additionally, it is supposed that C_{60} exists in the interstellar medium.[2,6] Our concern in this paper is to make use of the unique stability of C_{60} for photophysical investigations of large molecules.

The explanation of the photophysical processes that occur in C_{60} and other fullerenes promises to strengthen our general understanding of the interaction of photons with large molecules. Because C_{60} has a very rigid and highly symmetric molecular structure,[2] photophysical processes can be observed experimentally that have not been seen before. Even theoretical modeling of these processes with quasi-equilibrium theory is feasible since many parameters of this molecule, such as vibrational frequencies, bond

0022-3654/92/2096-10129$03.00/0

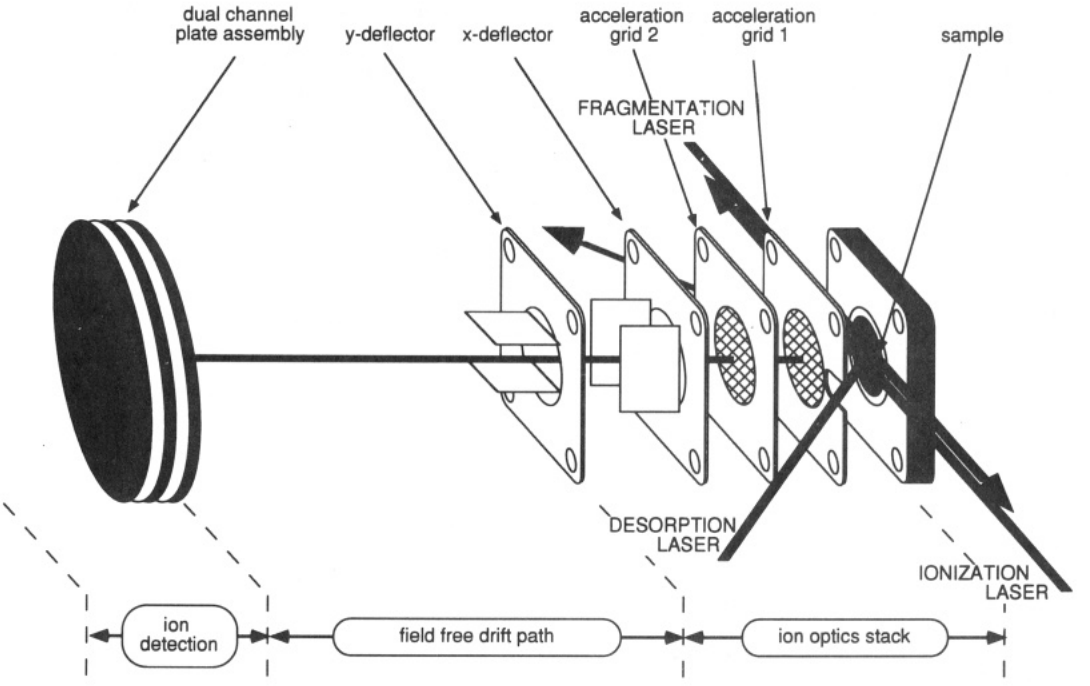

Figure 1. Schematic diagram of the laser desorption time-of-flight instrument. The sample is introduced into the system via a rapid sample transfer facility. The sample is typically at 8 keV. The first grid is at 7.6 keV, and the second grid is at ground potential. The molecular beam is directed between the sample surface and the first grid and is perpendicular to the laser beams for fragmentation and ionization. For the detection of neutral fragments from photodissociation, laser desorption of C_{60} from a solid sample was utilized. The desorption laser impinges the sample at ≈77° with respect to the surface normal. The 308-nm fragmentation laser and the 118-nm ionization laser beam counterpropagate parallel to and 2 mm above the C_{60} sample. Relative delays between the three lasers are independently adjusted for maximum signal.

distances, and ionization potentials, are known. This would be too complicated for a regular (that is, much less symmetric) molecule of comparable or larger size. Nevertheless, this will enable us to apply these findings to understand the ionization of very large molecular systems, such as biological species and nanomaterials, which is still a problem up to now.

This paper is an extension and completion of preliminary work previously published as letters.[7,8] In those letters, we reported on two of the most important channels accessible to C_{60} after multiphoton absorption: delayed ionization and neutral fragmentation. Both processes are basically methods of "cooling" a superheated molecule. In the first process, delayed ionization, C_{60} ejects an electron long after the multiphoton absorption by the molecule. This "thermionic emission" is a major ionization channel for C_{60} and C_{70}, and also for the larger fullerenes.[9] The second channel, neutral fragmentation, has not been studied in detail for these large molecules. In the past, most researchers have assumed that multiphoton ionization occurs in a stepwise "ladder-switching" process;[10,11] that is, the molecule becomes ionized with the first few photons and, if the molecular ion absorbs additional photons, fragmentation will follow. We have evidence that, at least for C_{60}, the neutral molecule absorbs 10–20 photons to form a superexcited (that is, internally hot) molecule, although 2–3 photons are sufficient to achieve multiphoton ionization. Furthermore, this superexcited molecule still fragments into neutral species. In this paper, we discuss the experimental observations of each of the decay channels of the superexcited molecule. In addition, theoretical models are invoked to describe the results. In particular, quasi-equilibrium theory is employed to model the two major decay channels of the superexcited molecule, fragmentation and delayed ionization, in terms of unimolecular decay and thermionic electron emission. Whereas the unimolecular decay is a standard application of the quasi-equilibrium theory (also known as RRKM theory),[12] the thermionic electron emission is the first application of a recently published theory.[13]

Experimental Section

The instrument used for these experiments is a laser desorption/laser ionization mass spectrometer that has been discussed in detail before.[14] Figure 1 shows the schematic diagram of this instrument. The mass spectrometer is a linear time-of-flight (TOF) instrument of 120-cm length. Particles are removed from the sample by a pulsed desorption laser and postionized with a second laser. An additional laser will precede the postionization laser to study the laser-induced dissociation of the desorbed molecules. An effusive source generates molecular beams of C_{60} for improved signal stabilities, necessary in selected experiments. The effusive source is a Ta cup (6.3-mm diameter, 8-mm length) with an aperture of 0.5 mm on one end. It is resistively heated and the temperature is monitored with a Chromel/Alumel thermocouple. The Ta cup is filled with approximately 200 mg of pure C_{60} (>99%). C_{60} is synthesized and purified in our laboratory according to published procedures.[3,15,16] The effusive source is operated at a temperature of ≈800 K, which corresponds to a vapor pressure of $\approx 5 \times 10^{-4}$ Torr[17] in front of the aperture and 3×10^{-7} Torr in the interaction volume.

The generated ions are brought to drift potential (8 keV) by a two-stage acceleration field. Ion detection is accomplished with a dual channel–plate assembly at moderate postacceleration potential (−2 kV). Data are recorded in a transient recorder with a maximum time resolution of 5 ns. Further processing of the data is accomplished in a PC-based software system. The typical operating vacuum is 2×10^{-9} Torr. The maximum mass resolution ($m/\Delta m$) of the instrument is approximately 1500 (fwhm at 720 amu), using a 5-ns laser pulse.

The 532-nm focused output of a Q-switched, mode-locked Nd^{3+}:YAG laser (the macropulse of 532-nm picosecond pulses of ~100-ps pulse duration each) is used for desorption of C_{60} from a solid sample deposited onto a stainless steel substrate. Postionization is performed with either a XeCl excimer laser (308 nm, 4.03 eV) or a harmonic frequency from a second Q-switched Nd^{3+}:YAG laser (the second to ninth harmonic, 532–118-nm wavelength, 5-ns pulse duration). The 118-nm light (vacuum-UV radiation) is produced by frequency tripling the third harmonic of a Nd:YAG laser in a gas cell filled with a Xe/Ar mixture.[18] The 118-nm beam is spatially separated from the 355-nm laser beam using the dispersion of a MgF_2 lens, and the 355-nm laser beam is deflected out of the apparatus with a translatable mirror

TABLE I: List of the Most Important Processes Occurring after Multiphoton Excitation of C_{60}[a]

$C_{60} + n(h\nu) \rightarrow C_{60}^+ + e^-$		direct ionization
$\rightarrow (C_{60})^*$	$\rightarrow C_{60} + h\nu'$	photon emission
	$\rightarrow C_{58}^+ + C_2 + e^-$	fragmentation (ions)
	$\rightarrow C_{58} + C_2$	fragmentation (neutrals)
	$\rightarrow C_{60}^+ + e^-$	delayed ionization
	$\rightarrow C_{58}^+ + C_2$	delayed fragmentation
	$\downarrow$	
	$C_{56}^+ + C_2$	sequential fragmentation
	$\downarrow$	
	$C_{54}^+ + C_2$	sequential fragmentation
	$\rightarrow C_{60-2n}^+ + C_{2n} + e^-$	fragmentation via C_n loss

[a] Direct ionization is probably limited to single-photon ionization and occurs only to a minor extent after multiphoton absorption. Multiphoton absorption results in the formation of the superexcited molecule C_{60}^* that is the precursor for the observed processes.

(high reflector at 355 nm) in vacuum. The lasers are triggered independently, allowing their relative timing to be adjusted. An iris is used to pick out the central portion of the desorption laser beam. A series of neutral density filters, or a $\lambda/2$-plate/polarizer combination, is used to keep the beam intensity below the desorption threshold for positive-ion production.[19] The desorption laser is obliquely incident on the sample ($\approx 70°$ with respect to the surface normal). The desorption energy is typically less than 0.01 mJ/pulse with an irradiated area of $<10^{-3}$ cm^2. The position of the desorption laser spot is monitored in real time with a video camera. The ionization laser intensity can be continuously varied using a set of mirror-image beam splitters (one high reflector at a specified wavelength, one uncoated) rotated in opposite senses to keep the beam from deviating in position and direction. The ionization laser exits the apparatus through a fused silica window, and the pulse energy is continuously monitored for fluence dependence studies. The size of the ionization volume was measured by splitting off a few percent of the ionizing light before entering the vacuum chamber and imaging the ionization spot on burn paper at the proper distance. The ionization laser is collimated in the ionization region.

Results

When laser light interacts with neutral C_{60} molecules in the gas phase, a variety of processes will occur. In Table I, we summarize most of the processes that are of importance in this kind of experiment. Experimental data will be presented for the channels accessible by our instrument.

The three major processes occurring after absorption of several photons by gas-phase C_{60} molecules are direct ionization, dissociation into ionic and neutral fragments, and delayed ionization.[20] We have recently attributed delayed ionization to thermionic emission of electrons from hot C_{60} molecules.[7] In the case of fragmentation, only even-numbered ion fragments are observed in the range between C_{60} and C_{32}.[20,21] The neutral low-mass fragments are assumed to be C_2 and C_{2n} molecules,[21,22] although this conjecture still awaits experimental confirmation. In addition to ionic fragments observable in the range between C_{60} and C_{32} are neutral fragments resulting from the dissociation process, as we showed in our recent work.[8] Further important processes to consider are delayed fragmentation (similar to delayed ionization) and sequential fragmentation, that is, the ejection of C_2 units until the remaining molecular fragment has cooled down sufficiently to be stable on the time scale of our instrument. Of course, a neutral or ionic fragment can absorb an additional photon and also undergo one of the above-mentioned processes. Thus, it is very difficult to isolate these processes for the smaller fragments and we shall focus on C_{60} alone.

A. Multiphoton Ionization of C_{60}. We use a molecular beam of C_{60} from the effusive source to study multiphoton ionization. The molecular beam issuing from this source provides much better signal stability compared to laser desorption from a solid C_{60} sample, a technique we[20] and others[23] have used before. The laser beams intersect the molecular beam in the ionization region of the mass spectrometer. Since the ionization potential of C_{60} is 7.61 eV,[24] multiphoton absorption for ionization is necessary for

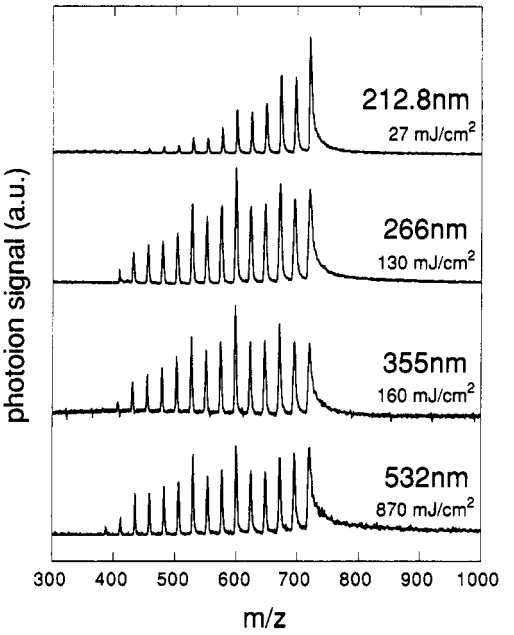

Figure 2. Time-of-flight spectra of photoionization of C_{60} provided from an effusive source. The mass peaks are the parent molecule C_{60} (on the right) and the even-numbered fragment clusters C_{58}, C_{56}, ..., down to C_{32}. Spectra have been selected for laser fluences that give approximately the same signal for the parent molecule at the detector.

photons of 212.8-, 266-, 355-, or 532-nm wavelength, requiring two, two, three, and four photons, respectively. Using these wavelengths, we always observe severe fragmentation of C_{60} accompanying the ionization. A distribution of fragment cluster ions down to C_{32}^+ is obtained. However, only even-numbered clusters are detected for fragment clusters consisting of 32 atoms or more.[20-22] Since the majority of smaller fragments (less than 32 atoms) is neutral and their ionization potentials are very high,[25] detection of these fragments has not been accomplished experimentally. It has been inferred from previous fragmentation studies that the major low-mass fragment is neutral C_2.[21,22] Intense fragmentation conditions also produce low-mass fragments, C_3^+ to C_{16}^+ of odd and even size, observable in comparable abundance to the larger fragments ($>C_{32}^+$). C^+ and C_2^+ are observed at much lower abundance.

Figure 2 displays photoionization spectra comparing the above-mentioned wavelengths with laser fluences selected to give approximately the same signal at the detector for the parent ion mass peak. Although different laser wavelengths (different number of photons required for ionization) and different laser fluences are employed, the measured spectra look very similar. Some propensity is found for fragments with "magic" numbers, presumably due to the more stable structures of these clusters, and fragmentation of C_{60} gives prominent yields of C_{50}^+ and C_{44}^+. Furthermore, the C_{60} ion peak shows a broadening toward longer flight times that is caused by delayed ionization.[20,23] This delayed ionization was first reported for metal clusters[26,27] and is attributed to thermionic emission of the highly excited molecule.[7] This will be discussed in detail later in the following section.

A summary of the dependence of the ionization of C_{60} on the fluence is presented in Figure 3. Ionization yields are compared for the whole wavelength range, including 118-nm light (single-photon ionization). The data are normalized for ionization volumes. For all wavelengths requiring multiphoton ionization, we observe a maximum in the fluence dependence, followed by a decrease in signal for higher fluences. This results from the competition of processes with different laser fluence dependence. At high laser fluences, fragmentation reduces the number of parent molecules available for ionization. Further increase of the laser fluence will lead to even more fragmentation, possibly until no parent ion is detected.

The dependence of the ion yield on the laser fluence should reveal the order of the multiphoton process. However, the slope

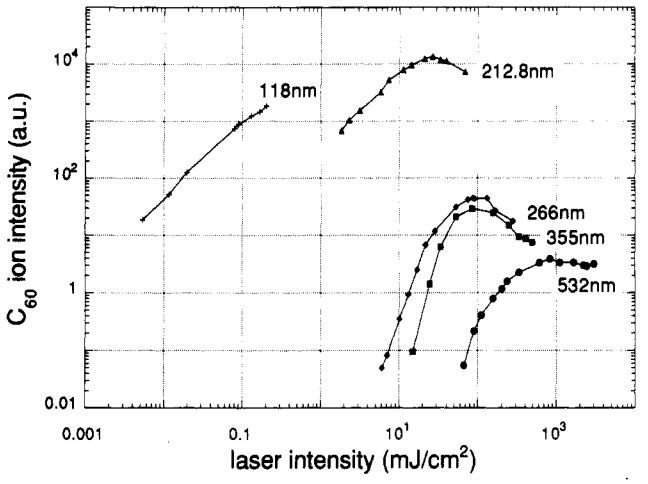

Figure 3. Comparison of the C_{60} prompt photoion yield dependence on the laser fluence for different ionization wavelengths. Actual ionization volume has been taken into account, which explains the different yields compared to Figure 2. The laser fluence for 118-nm light is measured indirectly by photoionization of acetone and calibrated with the cross section, thus introducing a considerable uncertainty by a factor of 5.

relates directly to the number of photons only for a true nonresonant process and will be lower for resonant and near-resonant transitions. Additionally, saturation effects will decrease the slope; thus it has to be extracted on the low fluence side. The initial slope for 266-nm light is approximately 4. For the longer wavelengths (355 and 532 nm) a slope of 5 is obtained, although three or four photons would be sufficient for direct ionization. This indicates that there are processes competing with multiphoton ionization. Basically, the electronic excitation is rapidly converted to internal excitation. As we show later, the actual number of photons that is absorbed is even larger.

For 212.8-nm light, a second-order process for ionization is also expected. However, ionization appears to be first order with the laser fluence, even at low fluences sufficiently far away from saturation. In addition, no fragmentation is observed in this fluence range. This indicates a one-photon process (Figure 3). This is possible, since the 800 K molecules from the effusive source already have 4.2-eV internal energy (see Theoretical Modeling) that may be available for ionization. A similar observation was made for ionization with 193 nm (6.42 eV), where a linear dependence of the ionization yield on the laser fluence was also found for hot C_n clusters.[28] This dependence changed to quadratic when cooler clusters were used. In our earlier publication on the fragmentation of neutral C_{60} molecules, we also found a first-order process.[20] Likewise, this resulted from initially hot neutral molecules brought into the gas phase by laser desorption at a temperature of ≥2000 K. Thus, ionization with 212.8-nm light is much more efficient than with the longer wavelengths (Figure 3). Also the absorption spectra of C_{60} in solutions show higher absorption at 212.8 nm, which is at the shoulder of the absorption peak at 211 nm, compared to the longer wavelengths.[29] Of course, the relationship of these absorption spectra in solution to gas-phase absorption spectra is so far unknown.

Figure 4 shows mass spectra for 212.8-nm ionization using different laser fluences for ionization. Negligible fragmentation and delayed ionization are observed for very low laser fluences. This behavior is never observed for longer wavelengths ($\lambda \geq 266$ nm). Considerable fragmentation and delayed ionization for all laser fluences is obtained for these wavelengths. Fragmentation-free excitation/ionization (no delays) is observed at all accessible laser fluences only for vacuum-UV light, either with 118 or 127 nm (Figure 5).[30]

The signal dependence on the laser fluence for the C_{60} ion and selected fragment ions, C_{58}^+, C_{50}^+, C_{44}^+, and C_{34}^+, is shown for ionization with 212.8- and 266-nm light in parts a and b, respectively, of Figure 6. The displayed signal intensities are integrated over the peak areas in the mass spectra. For C_{60}, this integral is split into two components, a prompt ($\Delta t \leq 100$ ns) and

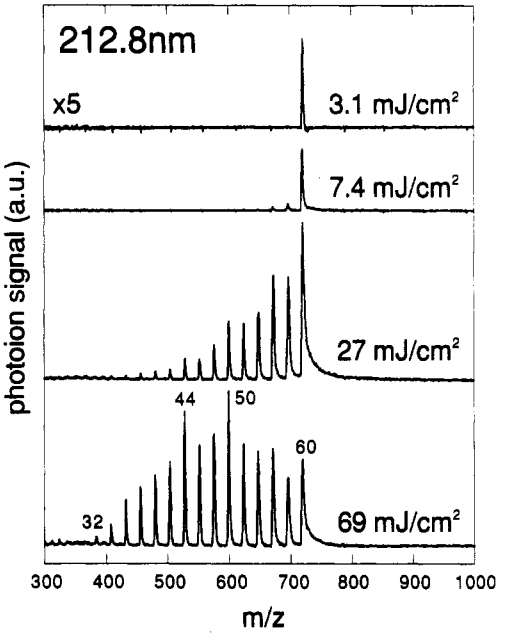

Figure 4. Laser ionization of C_{60} molecules provided from an effusive source by 212.8-nm light at various laser fluences. The C_{60} parent ion and the even-numbered fragment ions, C_{58}, C_{56}, ..., down to C_{32}, are identified.

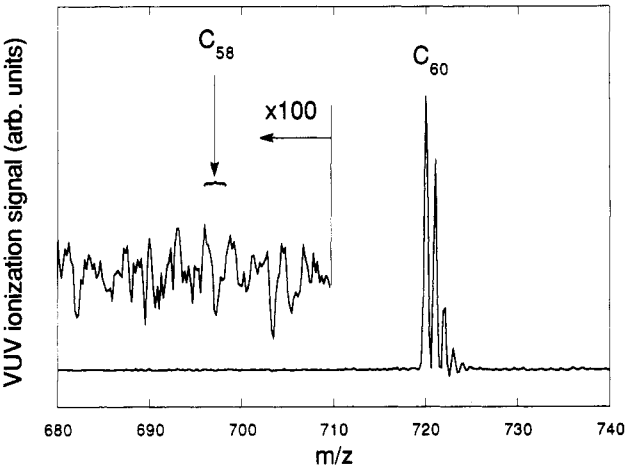

Figure 5. Postionization of laser-desorbed C_{60} with 127.53 nm (9.723 eV) from a tunable vacuum-UV laser. The absence of delayed ionization allows for high mass resolution ($m/\Delta m$ = 1500). Additionally, this vacuum-UV wavelength yields fragmentation-free ionization, as can be seen on the expanded scale.

a delayed contribution. Strong fluence dependences are observed for prompt ionization, delayed ionization, and fragmentation. All channels show very similar behaviors, implying a common precursor for these processes. The dependence on the laser fluence of these processes gives a slope ≥4, which is also only a lower limit for the number of photons required for these processes. The notable exception is prompt ionization of C_{60} with 212.8-nm light that appears to have a linear fluence dependence as explained above.

The fluence dependence for 355- and 532-nm ionization is very similar to that for 266 nm, although shifted to higher laser fluences. Fragmentation becomes the dominant channel at higher fluence. Even the yield of larger fragment ions decreases, whereas the smaller fragments still rise considerably. At very high laser fluences, fragmentation is by far the dominant process, which can easily be verified by adding up all fragment ion signals.

B. Delayed Ionization. As already mentioned above for multiphoton ionization of C_{60}, we distinguish between prompt and delayed ionization. Prompt ionization (or direct ionization) means that optical excitation directly excites a single electron above the ionization potential so that electron detachment occurs without

TABLE II: List of Identified Rates for Delayed Electron Emission from C_{60}[a]

	k_i (s^{-1})	A_i (AU)	internal energy (eV)	integral of delayed signal (AU)
wavelength, 212.8 nm;	1.8 (4)	1.18	34.2	65.4
photon energy, 5.826 eV	7.5 (5)	1.29	41.0	1.33
	2.8 (6)	4.23	43.9	1.51
	8.5 (6)	7.69	46.6	0.905
wavelength, 266.0 nm;	1.3 (5)	1.21	37.5	9.28
photon energy, 4.661 eV	1.0 (6)	1.90	41.4	1.9
	3.6 (6)	6.99	44.4	1.9
wavelength, 354.7 nm;	9.0 (4)	2.08	36.8	23.1
photon energy, 3.493 eV	6.8 (5)	4.59	40.6	6.75
	2.5 (6)	7.67	43.6	3.07
	8.6 (6)	15.0	46.6	1.75
wavelength, 532.0 nm;	1.0 (5)	0.433	37.0	4.33
photon energy, 2.331 eV	1.0 (6)	1.15	41.4	1.15
	4.5 (6)	2.10	44.9	0.467

[a] Signal tails of the C_{60} peak are fitted with a sum of exponentials of the form (least-squares fit) delayed signal = $\sum_i A_i e^{-k_i t}$. Internal energies are obtained from Figure 16. The numbers in parentheses are powers of 10 throughout the table. Also, the integral of the delayed signal for a particular rate, k_i, is given.

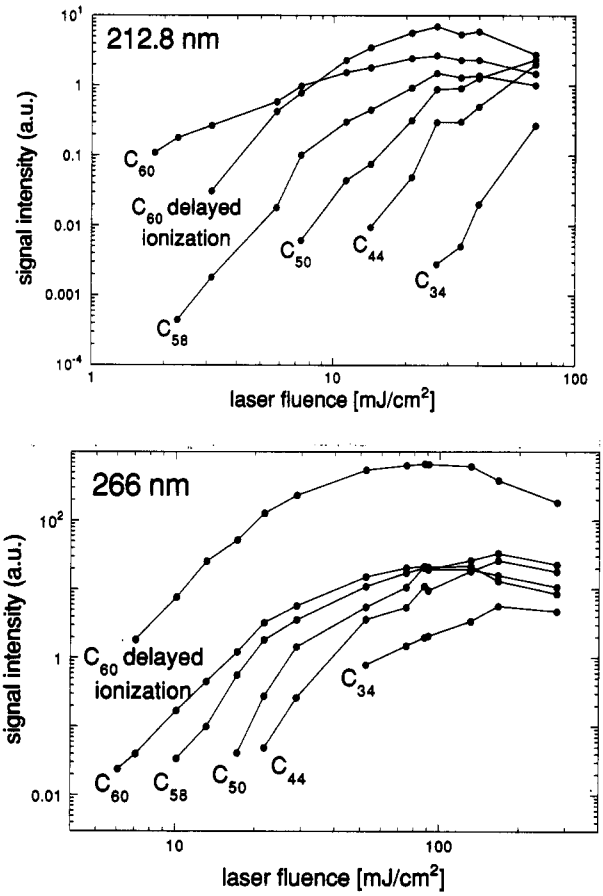

Figure 6. Signal dependence on laser fluence for the C_{60} ion and some representative fragment ions (C_{58}, C_{50}, and C_{34}) for ionization by (a) 212.8- and (b) 266-nm light. The displayed signal intensities are integrated over the peak areas in the mass spectra. For C_{60}, this integral is split into two components, a prompt and a delayed contribution, labeled "C_{60}" and "C_{60} delayed ionization", respectively.

observable delay on the time scale of these experiments (>100 ns). At higher laser fluences, delayed ionization is even more abundant than prompt ionization (Figure 6), especially for longer wavelengths (≥266 nm). Additional evidence for the observation of delayed ionization is the detection of the arrival time of the photoelectrons. In our apparatus, all photoelectrons produced are detected in the same way as photoions by switching the polarity of the acceleration voltages. The photoelectrons resulting from laser ionization are accelerated with 4 kV into the field-free drift tube, which is lined with μ-metal inside the vacuum chamber (no electron energy dispersion). A comparison of photoions and

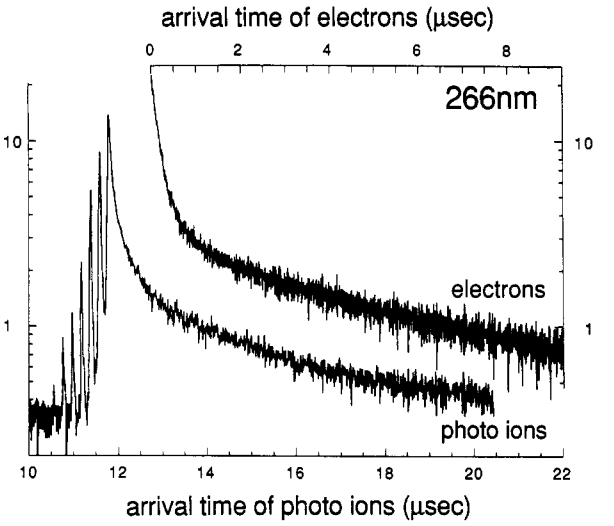

Figure 7. Time-of-arrival of photoelectrons and photoions for ionization of C_{60} with 266-nm laser light. The signal tails are identical for photoelectrons and photoions.

photoelectrons is depicted in Figure 7, showing *identical* tails for photoions and photoelectrons. Delayed ionization can be fitted by a sum of three to four exponentials for all wavelengths. A sequence of these fits is displayed in Figure 8. The rates for delayed emission range from 10^4 to 10^7 s^{-1}, limited by the observation time and time resolution of our instrument. A list of these rates for C_{60} is given in Table II. We find that the rates for delayed electron emission from C_{70} are in the same range as for C_{60} (3.5×10^5 and 4.0×10^6 s^{-1} at 270-nm wavelength). The rates remain unchanged over the whole fluence range for a particular wavelength but vary for different wavelengths. Furthermore, no dependence on the acceleration potential is found, thus precluding an instrumental artifact.

C. Neutral Fragments. So far, we have only described ion fragments after multiphoton absorption, implying that ionization precedes fragmentation and, hence, all fragments are ionized. However, we showed recently that this is not the only pathway for decomposition of C_{60}. There are also large neutral fragments with a similar distribution to the ion fragments.[8] The detection of neutral fragments after photoionization requires an additional laser that succeeds the fragmentation laser and ionizes the remaining neutral fragments. This laser may not cause additional fragmentation, which would make interpretation of the mass peaks in the spectrum impossible. Single-photon ionization attained with 118-nm light seems suitable for this task. In fact, single-photon ionization of laser-desorbed C_{60} (internal temperature >2000 K) yields no fragmentation.

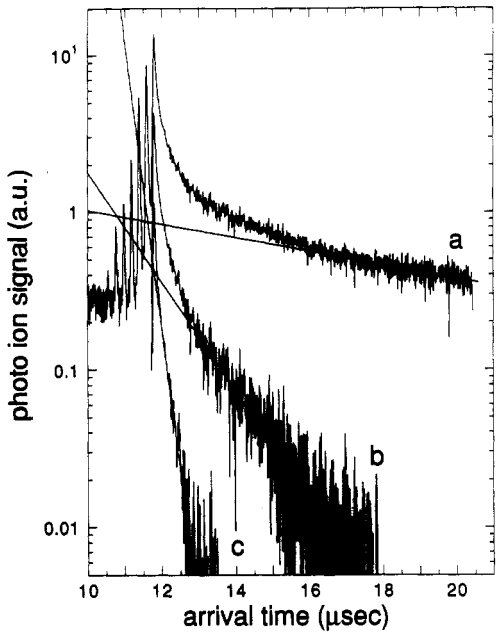

Figure 8. Sequence of determination of rate constants for delayed electron emission. (a) Time-of-flight spectrum of C_{60} and the fragment ions C_{58}, ..., C_{48} with 266-nm ionization as in Figure 6. (b) After subtraction of one exponential from spectrum a, offset by a factor of $^1/_3$. (c) After subtraction of two exponentials from spectrum a, offset by a factor of $^1/_{10}$. The straight lines are the exponentials that are subtracted.

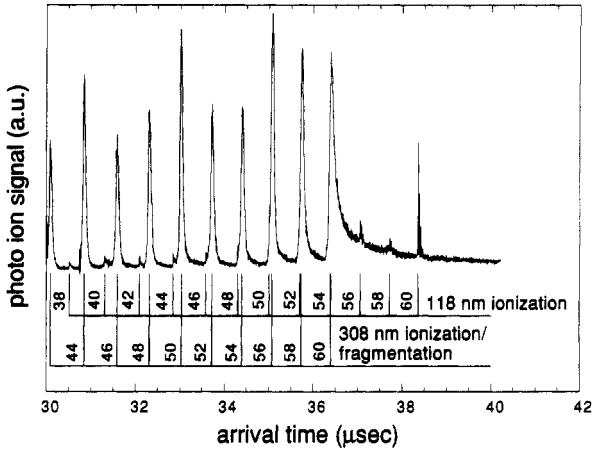

Figure 9. Time-of-flight spectrum of the three-laser experiment. Neutral C_{60} molecules are desorbed from the solid sample by a 532-nm laser pulse. In the gas phase, the molecules are subjected to an intense dissociation laser pulse (308 nm) and subsequently to an ionization laser pulse (118 nm). The time delay between the 308-nm laser and the 118-nm laser is approximately 1.8 μs. The ionic fragments and the neutral fragments from the 308-nm dissociation laser can be easily identified due to the delay of the 118-nm ionization.

Figure 9 shows the observed time-of-flight spectrum for this experiment. Neutral C_{60} molecules are desorbed from the substrate and are subjected first to a dissociating laser beam (308 nm), and after an appropriate delay of several microseconds, the remaining neutral molecules are ionized by the vacuum-UV laser. Since the vacuum-UV laser intensity is not sufficient to saturate the ionization of these molecules (Figure 3), only a fraction of the neutral molecules is ionized. The peaks originating from either photodissociation/photoionization with 308 nm or photoionization with 118 nm are labeled for clarity. The parent vacuum-UV ionization peak decreases by an order of magnitude when the dissociation laser is present, showing good spatial overlap of the two laser beams.

To alleviate the interference of the ion fragments from the dissociation laser, we pulsed these ions out electrically; that is, the extraction voltage is pulsed on following the 308-nm dissociation laser and immediately preceding the 118-nm ionization

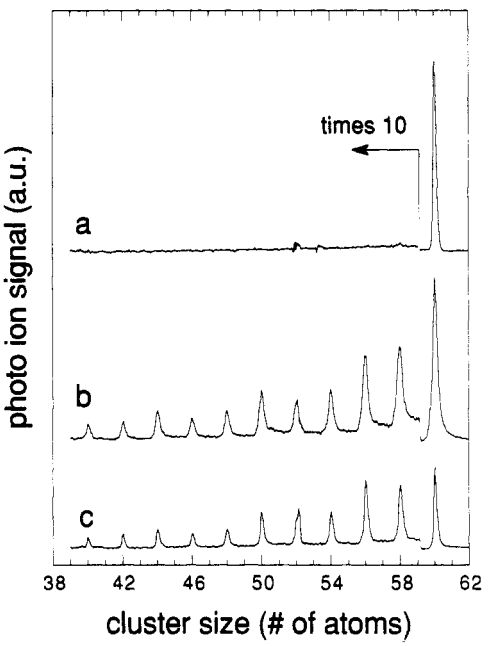

Figure 10. Spectra from neutral C_{60} molecules desorbed from the solid sample by a 532-nm laser pulse. (a) Time-of-flight spectrum using only 118-nm ionization of the desorbed molecules, showing that no fragmentation of C_{60} is caused by the vacuum-UV ionization. (b and c) Pulsing out the ions caused by the 308-nm dissociation laser and ionizing the remaining neutral molecules after a given delay time: (b) at 1 μs and (c) at 2 μs. Spectra b and c are at a larger vertical scale than spectrum a.

laser. The resulting spectra are depicted in Figure 10. The top trace shows postionization by the vacuum-UV laser (118 nm) without the dissociation laser to prove that this wavelength does not cause any fragmentation of C_{60}. In the lower panels, the dissociation laser precedes the vacuum-UV ionization by 1 and 2 μs, respectively. The parent molecular ion, C_{60}^+, is the most intense peak in the spectra since the 308-nm radiation does not ionize/dissociate all of the C_{60} molecules. With longer delay times, we observe a weakening in signal due to the two-dimensional expansion of the interaction volume with respect to the ionization laser. The distribution of neutral fragments looks very similar to the distribution of ion fragments (compare with Figure 2). Not much qualitative change in the distribution of fragments for increasing delay time can be observed, although the smaller fragments seem to decrease in signal faster than the larger ones. This indicates that fragmentation is much faster than the microsecond time scale we are probing here.

Unfortunately, the energy of 10.5 eV provided by the vacuum-UV photon (118 nm) is not sufficient for the ionization of carbon atoms and C_2, C_3, C_4, and C_5 clusters, since the respective ionization potentials are 11.0, 12.1, 11.4, 10.5, and 10.7 eV.[25] Therefore, for the detection of the low-mass neutral fragments, one has to resort to resonant photoionization techniques that are currently under development in our laboratory. Our preliminary results show that carbon atoms are detected as fragmentation products of C_{60}. Since we use a 2+1 resonance ionization scheme to detect carbon atoms,[31] it is not clear if we do not dissociate the C_2 and C_n fragments to carbon atoms in the course of resonant ionization. Further work on this topic will be presented in a forthcoming publication.[30]

Theoretical Modeling

We strongly believe that the observed processes, delayed ionization and fragmentation, are thermally induced. The reasons are that there is minimal wavelength dependence for delayed ionization and fragmentation, there is very similar fluence dependence in all the channels, and the slopes indicate higher order processes than would be expected for simple multiphoton ionization. The energy provided by the absorbed photons is converted to internal excitation at a rapid rate, heating the molecule to

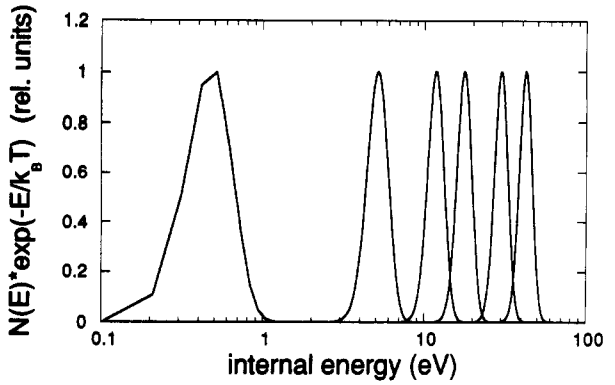

Figure 11. Vibrational energy distributions of gas-phase C_{60} at 300, 900, 1500, 2000, 3000, and 4000 K from left to right, respectively.

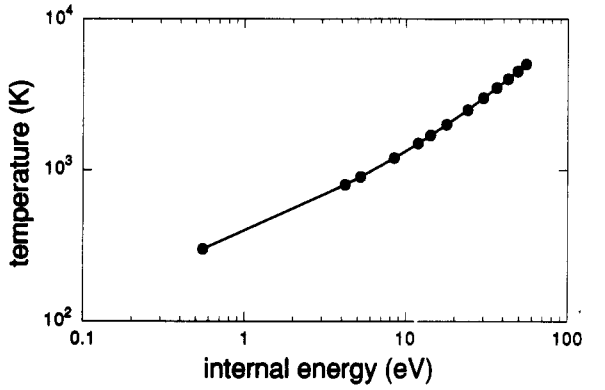

Figure 12. Relationship of temperature and average vibrational internal energies for C_{60}.

significant temperatures. The obvious choice to model a thermally-activated process is to use quasi-equilibrium theory to calculate the rates for these processes.[12]

For the calculation of the density of states, we modified the calculated vibrational frequencies from Stanton and Newton for neutral C_{60}[32] so that they reproduced the reported experimental values.[33] The density of vibrational energy levels and the integrated densities of states are calculated by using the Haarhoff approximation.[34] For icosahedral point group, I_h, the symmetry factor, σ_i, that goes into the rotational partition function is 60. Figure 11 displays the vibrational energy distribution ($N(E)e^{-E/kT}$) for various temperatures. At 300 K, the average internal energy is already ≈0.5 eV. At the temperature of the effusive source, 800 K, the average internal energy is 4.2 eV. For laser desorption of neutral C_{60} from the solid sample, the molecules have a whopping 20 eV of average internal energy. The relationship between the average vibrational energy and the temperature is given in Figure 12.

A. Thermionic Emission Model. We follow the adaptation of quasi-equilibrium theory as outlined by Klots for the delayed ionization[13] to derive the rate constant, $k(E)$, of electron emission from a molecule with internal energy, E.

$$k(E) = \frac{W(E,D_0)}{h\rho(E)} \tag{1}$$

h is Planck's constant, $\rho(E)$ is the density of states of C_{60}, and

$$W(E,D_0) = \int_0^{E-D_0} \rho^*(\chi)\, d\chi\, (1 + (2\pi/h)[2\mu b^2(E - D_0 - \chi)]^{1/2})^2 \tag{2}$$

where μ is the reduced mass (≈electron mass), b is the classical hard-sphere collision radius (5.0 Å), D_0 is the activation energy (energy threshold for electron ejection), and $\rho^*(E)$ is the density of states for the activated complex. For large species, this becomes the Richardson–Dushman equation for thermionic emission.[35] In the calculation, we assume that the vibrational frequencies of C_{60} remain the same after electron emission. Furthermore, we take

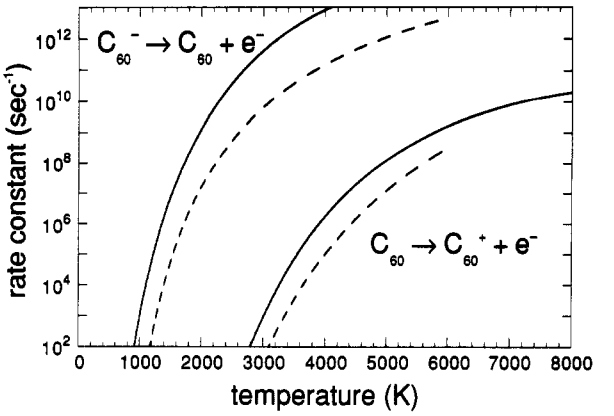

Figure 13. Calculated rates for delayed ionization of C_{60} and delayed electron detachment of C_{60}^- (as labeled in figure) using quasi-equilibrium theory (full lines) and the Richardson–Dushman equation (dashed lines). The relationship between temperature and internal energy is derived from Figure 12.

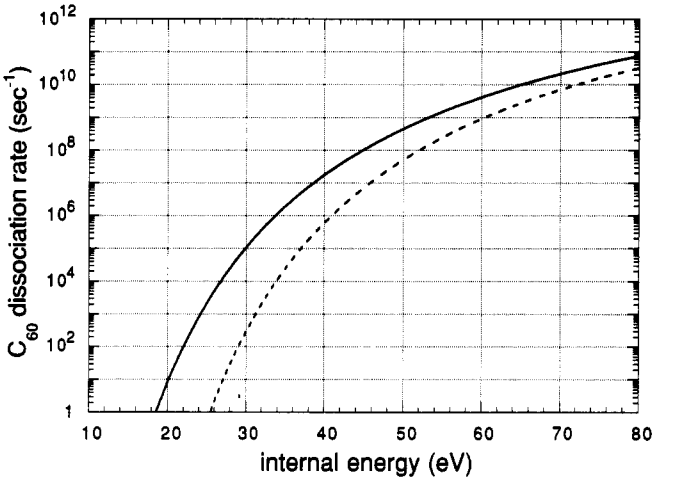

Figure 14. Rates of unimolecular decay of C_{60} (solid line) using an activation energy of 4.6 eV and a reaction coordinate of 1050 cm^{-1}. The dashed line is a simple RRK calculation for the same process using ν = 1000 cm^{-1}.

7.61 eV, the known ionization energy of C_{60},[36] as the activation energy D_0 for this process. The same formalism can be applied for delayed electron detachment from C_{60}^-, using the electron affinity of C_{60}, 2.65 eV,[37] as the activation energy. Figure 13 shows the calculated rate constants for these processes. In addition, a calculation of the thermionic emission rate, using the Richardson–Dushman equation,[35] is provided.

$$k_{RD}(T) = ACT^2e^{-\phi/k_BT} \tag{3}$$

k_{RD} is the rate constant of electron emission (actually, this is the current), A is the surface area of the electron emitter, C = 120.4 C s^{-1} cm^{-2} K^{-2} is the "universal constant", ϕ is the work function, k_B is the Boltzmann constant, and T is the absolute temperature. The agreement with quasi-equilibrium theory is reasonable, considering that the Richardson–Dushman equation is derived for macroscopic samples. Since the surface plays a more important role for a finite size electron emitter,[13] the rate constant for electron emission rises for smaller entities, consistent with our results displayed in Figure 14. Electron detachment of C_{60}^- is a very fast process compared to thermionic emission from C_{60}. For our experimental conditions, we get $k \approx 10^7$ s^{-1} at 2000 K, which is the approximate temperature of C_{60} after laser desorption.[20] In our instrument, we observe that most of the C_{60}^- ions are neutralized after the acceleration stage on the way to the detector. This is measured by deflecting the ions out of the field-free drift region at half of the distance to the detector (after ≈20 μs); thus the observed signal represents neutral molecules. Applying the Richardson–Dushman equation, Wang et al.[37] concluded that it

TABLE III: Quantities Listed as a Function of Energy, E; Density of States, $N(E)$; Number of States for the Activated Complexes for Delayed Electron Emission, $G_e^*(E-D_0)$, and Unimolecular Decay, $G_f^*(E-D_0)$, with the Activation Energies 7.61 and 5.6 eV, Respectively; Rates for Delayed Electron Emission, $k_e(E)$, and Unimolecular Decay, $k_f(E)$[a]

internal energy (eV)	$N(E)$ (J^{-1})	$G_e^*(E-D_0)$	$G_f^*(E-D_0)$	$k_e(E)$ (s^{-1})	$k_f(E)$ (s^{-1})
10	2.65 (114)	6.71 (45)	4.32 (62)	1.42 (-11)	4.27 (-17)
20	1.52 (149)	5.63 (104)	7.5 (111)	2.80 (-2)	5.19 (-3)
30	3.95 (172)	1.04 (136)	3.5 (140)	8.67 (2)	6.51 (2)
40	1.60 (190)	7.87 (157)	8.58 (160)	4.48 (5)	3.75 (5)
50	3.83 (204)	4.42 (174)	1.20 (177)	2.78 (7)	2.01 (7)
60	4.44 (216)	2.96 (188)	2.26 (190)	4.88 (8)	3.09 (8)
70	8.76 (226)	1.43 (200)	4.33 (201)	3.88 (9)	2.24 (9)
80	1.23 (236)	1.89 (210)	2.79 (211)	1.63 (10)	1.03 (10)
90	1.77 (244)	1.31 (219)	1.10 (220)	3.39 (10)	3.44 (10)

[a] The transition state for the unimolecular decay is taken as 1050 cm^{-1}, and the reaction path degeneracy $\alpha = 30$. The numbers in parentheses are powers of 10 throughout the table.

takes about 14 eV (that is, four 353-nm photons) to induce substantial electron emission from C_{60}^- on a microsecond time scale, a result that is in good agreement with our calculation.

B. Unimolecular Decay Model. To calculate the rate, $k_f(E)$, of unimolecular decay of C_{60}, we used the well-known equation given in ref 12

$$k_f(E) = \frac{\alpha G^*(E-D_0)}{hN(E)} \tag{4}$$

where α is the reaction path degeneracy, h is Planck's constant, $G^*(E-D_0)$ is the number of states of the activated complex, and $N(E)$ is the density of states. There are 60 C–C bonds that establish a hexagon–pentagon edge and 30 C–C bonds that establish a hexagon–hexagon edge on the icosahedral cage. Removing a C_2 unit from the latter location results in a more symmetric fragment molecule, C_{58}, and also preserves the double bond. This process has a reaction path degeneracy $\alpha = 30$. As a first try, we used 4.6 eV for the activation energy in order to check against published results.[38,39] In addition, we chose 1050 cm^{-1} as reaction path coordinate, a value between the two extremes 263 and 1722 cm^{-1} employed by Yoo et al.[39] Our result falls nicely between the two extreme cases studied in ref 39, since we used an intermediate reaction path coordinate. Also, the classical expression (RRK theory) is evaluated for the same activation energy and is added to Figure 14.

$$k_{cl}(E) = \alpha\nu(1 - D_0/E)^{s-1} \tag{5}$$

α is the reaction path degeneracy, ν is the frequency factor, D_0 is the activation energy, and s is the number of vibrational degrees of freedom. With $\nu = 1000$ cm^{-1} and the other parameters as given above, we obtained the result depicted in Figure 14.

Using 4.6 eV for the activation energy, as suggested by Radi et al.,[38] gives rates for fragmentation that are much too high to explain our experiment. Since delayed ionization and fragmentation always occur together, they should have comparable rates. Yoo et al.[39] also suggested higher activation energies for the unimolecular decay process based on their observations. On the other hand, at least 7.2 eV are necessary to remove a C_2 unit from a pure carbon lattice.[38] A similar kind of reasoning gives 7.6 eV for the removal of C_2 from C_{60}.[39] These values seem somewhat too high to explain our data.

C. Comparison of Experiment to Theory. The density of states of C_{60} and the integrated density of states for the activated complex are both very large. Some of the calculated values are reproduced in Table III. The dependence of the density of states and the integrated density of states for the activated complex on the vibrational frequencies is strong. However, it influences the rate constants only to a minor extent. The crucial parameter is the activation energy for the process. Each additional electronvolt for the activation energy decreases the rates by several orders of magnitude (Figure 15). We choose 5.6 eV for the activation energy for unimolecular decay based on our experimental observations. The final calculations of the rate constants for delayed electron emission and fragmentation are both depicted in Figure 16. The experimental rate constants for delayed electron emission are indicated by circles on the corresponding curve so that vibrational energies of the excited molecule can be derived. These energies fall in the range 34–47 eV. Since not every C_{60} molecule absorbs the same number of laser photons, there will be a distribution of internal energies. A thermal distribution of the vibrational energy is displayed for 4000 K in Figure 16. The actual energy distribution will differ from the thermal distribution mainly in a lower density at higher energies, as calculated for CF_3I.[40] Higher laser fluences, that is, the absorption of more photons by the molecule, will lead to further heating and consequently shift the internal energy distribution to higher energies. Thus, fragmentation will become more important than delayed ionization.

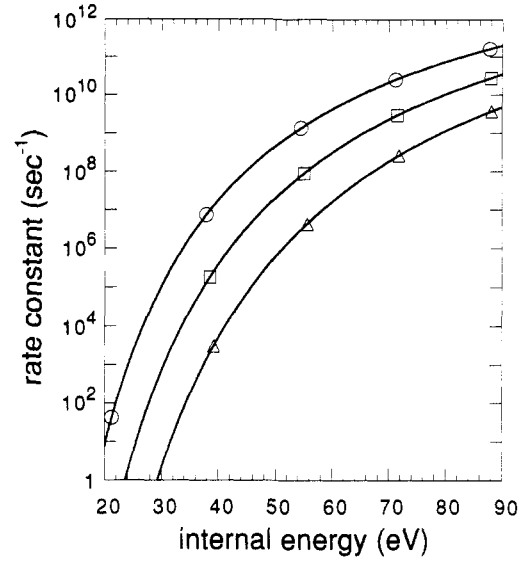

Figure 15. Rates of unimolecular decay of C_{60} using activation energies of 4.6 (top curve), 5.6 (center curve), and 6.6 eV (bottom curve). The reaction coordinate is 1050 cm^{-1}.

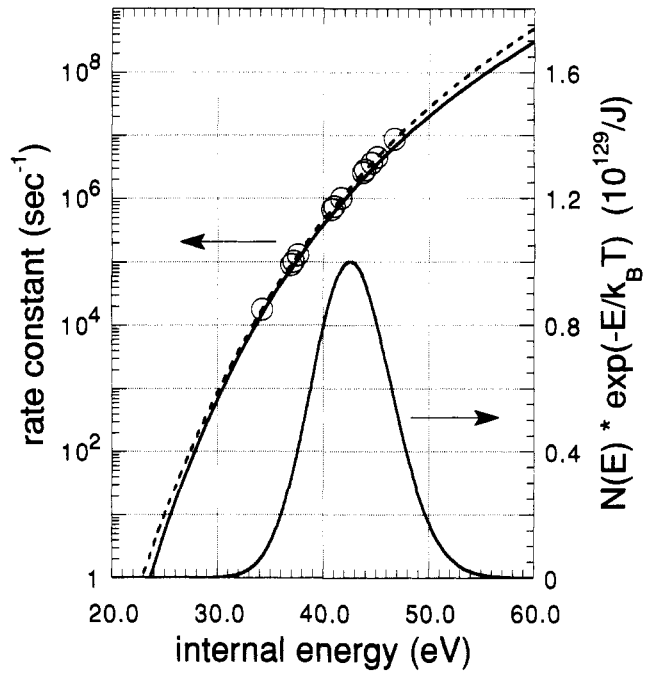

Figure 16. Rate constants from RRKM theory for thermionic emission of electrons (dashed line) and fragmentation (full line) of excited C_{60}. The activation energies are 7.61 and 5.6 eV, respectively. The observed rate constants for delayed electron emission are indicated (open circles). Furthermore, the internal energy distribution at 4000 K is given (use right-hand scale).

This is borne out by observations in the present experiments (Figures 3, 4, and 6).

The quasi-equilibrium theory calculation, together with our experimental evidence, implies that the excitation to high internal energies is the common cause for the observed processes. Let us review the reports of experimental data and theoretical calculations from other groups pertaining to our study. In a gas-phase collision study of C^+ ions with C_{60} vapor, the fragmentation rate of C_{60} is measured in the energy range of 2–78 eV.[41] The dependence of the yield of various ion fragments (C_{58}^+, C_{56}^+, to C_{44}^+) on the collision energy is another demonstration of the stability of C_{60}. Significant yield of the fragment ion C_{58}^+ is observed in the energy range of 30–40 eV. The yields of the lower fragments C_{56}^+ to C_{44}^+ are shifted to higher collision energies by ≈6 eV each with respect to the next larger fragment size. This implies that an energy of approximately 6 eV is necessary to remove a C_2 unit from the cage, which is in good agreement with our choice of activation energy for fragmentation of 5.6 eV. A vacuum-UV photoionization study showed that at least 40.8-eV photon energy is necessary to observe fragmentation of C_{60} in their instrument.[39] In an ion beam scattering experiment of C_{60} on graphite, further evidence of the resilient structure of C_{60} is reported.[42] No fragmentation was found for impact energies up to 170 eV. This was already realized from a computer simulation,[43] predicting that C_{60} should withstand collisions on diamond up to about 200-eV kinetic energy. In addition, approximately 50 eV of the original kinetic energy is transferred into internal motions of the rebounding molecule. In a recent theoretical paper MNDO calculations of the enthalpy changes for fragmentation of C_{60} are reported.[44] It is found that, for the process $C_{60} \rightarrow C_{58} + C_2$, 11.8 eV are needed, which is higher than everything mentioned above. However, the author considers the fragmentation process as proposed by O'Brien et al.,[21] where the C_2 molecule leaves from a pentagon–pentagon edge. This involves transformation of the icosahedral C_{60} molecule to an isomer as a first step before ejection of a C_2 molecule. This requires 1.9 or 3.79 eV, depending on the isomer, respectively.[44] Furthermore, for the transformation to the first isomer an activation barrier in excess of 5 eV has been calculated.[45] Thus, we conclude that the ejected C_2 from C_{60} does not originate from a pentagon–pentagon edge, as put forward by O'Brien et al.[21]

Discussions

We have shown that C_{60} has to be excited to energies on the order of 50 eV to explain the observed processes. According to quasi-equilibrium theory of unimolecular decay, to break the weakest molecular bond, the vibrational energy of the molecule has to concentrate in this bond by fluctuation. Considering the many degrees of freedom and the high stability of C_{60}, the rate constants are very small for energies around the dissociation energy and high internal excitations are possible. Achieving these high internal excitations that are responsible for fragmentation as well as delayed ionization needs many more photons than would be needed for direct multiphoton ionization of C_{60}. Furthermore, to absorb approximately 10 photons, conversion from electronic excitation to internal excitation has to be very fast and fluorescence should be weak. The singlet-state lifetime is found to be 650 ± 100 ps,[46] reflecting indeed a fast intersystem crossing and weak fluorescence.

The dependence of the ionization on the laser fluence should reveal a multiphoton process of that order. Ionization and fragmentation appear to be of fourth to fifth order (Figures 3 and 6). However, in our case, we have absorption in the vibrational quasi-continuum of the molecule after the first few photons are absorbed;[47] thus most of the absorption events should be near-resonant. This implies that the "bottleneck" for multiphoton absorption occurs with the first (few) photon(s).

The possibility of highly excited molecules by IR radiation has been discussed by Letokhov.[47] The author gave a crude estimate for how much overexcitation, that is, excitation energy, E, in excess of the dissociation limit, D_0, is necessary to obtain unimolecular decay observable in experimental situations (constants $k = 10^7$–10^8 s^{-1}):

$$E + E_0 = D_0(1 - (W_{exc}/\bar{\omega})^{1/(s-1)})^{-1} \quad (6)$$

E_0 is the zero-point vibrational energy of the molecule and s is the number of vibrational degrees of freedom. The frequency coefficient is

$$\bar{\omega} = (\prod_{i=1}^{s} \omega_i)/(\prod_{i=1}^{s-1} \omega_i^*) \quad (7)$$

with the vibrational frequencies of the molecule, ω_i, and of the activated complex, ω_i^*. At the fluence giving maximum ionization yield (for 266 nm, $I = 100$ mJ/cm^2; see Figure 3), the excitation rate is $W_{exc} = \sigma I/E_\omega = 1.34 \times 10^{10}$ s^{-1}, with $\sigma = 2.9 \times 10^{-16}$ cm^2 (at 257 nm[48]), $\bar{\omega} = 9.45 \times 10^{14}$ s^{-1} (eq 7), and $I = 2 \times 10^7$ W/cm^2 at the photon energy, $E_\omega = 4.66$ eV. In our case, $E + E_0 = 15.3D_0$ corresponds to 71-eV excitation energy. This is an overestimation compared to our more elaborate calculations, although not surprising, since eq 6 is a modified form of the simple RRK theory that underestimates the rate constant (see Figure 14).

The calculated rate constants for thermionic electron emission from C_{58} are higher than those for C_{60} (factor of ≈10), even after taking into account the energy loss by the dissociation. Additionally, it is expected that the rates are even higher for the smaller fragments considering the increased importance of the surface. Thus, it is conceivable that all the ion fragments are formed by thermionic emission and neutral fragments are formed initially. This assumes that the fragment molecule does not absorb an additional photon that ionizes it. On the other hand, these fragments are already internally hot so the conversion to internal energy should be very fast compared to ionization, and the absorbed photon will add to the internal energy. This could also be true for ionization of the parent molecule. At least for excitation with long wavelengths (266–532 nm) the distinction between direct ionization and delayed ionization could be a result of the resolution of our instrument. For these wavelengths we always observe delayed ionization even at very low laser fluences, in contrast to 212.8-nm light where for low laser fluences the single-photon process dominates and a distinction between direct and delayed ionization is easily possible.

The measured rates for delayed electron emission seem to exhibit some grouping around certain energies. This has yet to be explained. Any memory of the first excitation should be entirely lost because of the fast intramolecular vibrational energy redistribution, especially for these highly excited molecules.[49] We suggest that this may be caused by different isomers of C_{60},[50] which might have ionization potentials different from icosahedral C_{60}, as a calculation for one isomer showed.[45] Another possibility for this grouping could be that different photon energies access different autoionization states in the continuum.

As for the whole distribution of fragments, this can be understood in the form of a stepwise process. The removal of one C_2 unit reduces the internal energy of C_{60} by at least ≈6 eV. C_{58} has a higher rate for unimolecular decay but also less internal energy than its parent. This process will continue until the fragment arrives at an energy where the fragmentation rate at the remaining energy is small. The initial excitation determines the number of steps for this process; thus, a distribution of initial energies will lead to a distribution of fragments. In other words, the excited molecule boils off C_2 units until the final product molecule has cooled sufficiently to be stable enough for detection on our time scale. Larger units may even be emitted (C_4, C_6, or C_8, ...) as inferred from an ion fragmentation study.[21] The MNDO calculations by Stanton[44] show that the concerted elimination of a C_4 or C_6 unit is energetically favored over the sequential loss of C_2 units. The whole distribution of fragment ions, therefore, reflects the original excitation of the molecule, convoluted with the different stabilities of these fragments. Moreover, thermionic emission is just another pathway for energy loss, that is, boiling of an electron from C_{60} or a fragment molecule. These C_{60} ions could originate from the low-energy tail of the internal energy distribution with the higher excited molecules fragmenting. This

agrees well with the interpretation of the rates of delayed electron emission presented in Table II, where the C_{60} ion signal is more abundant at lower emission rates, that is, lower internal energy.

Finally, let us consider radiation cooling of the molecule, a possible process we also listed in Table I. An entity at a temperature of 4000 K should emit significant blackbody radiation. However, the spectral emissive power of the blackbody, given by Planck's law, has to be reduced to take into account the size of the emitter with respect to the emitted wavelength.[51] The maximum of the blackbody emission is at a wavelength of 725 nm at that temperature. For silver clusters consisting of 1000 atoms, the blackbody emissive power is reduced by a factor of 2.67×10^{-4}.[51] Thus, the energy emitted from a hot C_{60} molecule during 1 μs would be much less than 1 eV. However, for longer observation times on the order of milliseconds, photon radiation has been considered an effective pathway for cooling.[52] Presumably, this occurs by emitting IR photons near the IR-active vibration modes rather than blackbody emission.

Conclusions

We showed that C_{60} absorbs 10–20 laser photons, although only a few photons of the applied wavelength would be required for multiphoton ionization. The electronic excitation is converted to internal excitation of the molecule, facilitated by the high number of degrees of vibrational freedom and the resulting enormous density of states. Thus, the parent molecule undergoes severe fragmentation and delayed ionization, both processes indicative of high internal excitations. Quasi-equilibrium theory is employed to model fragmentation and delayed ionization and determines the energy range where these processes take place. The obtained results agree with related experiments.

The effect of excitation of the molecule to high internal energies by IR lasers has been summarized by Letokhov.[47] Our findings extend the applicable range of this theorem to visible and even UV laser light for sufficiently large molecules. This has serious consequences for the use of multiphoton postionization techniques to detect large molecules. If C_{60} were not so rigid, fragmentation or even total decomposition would have taken place at these energies, long before any parent ion or large-ion fragment could be detected mass spectroscopically. An experiment that supports this assumption has been presented recently.[53] The authors showed that, for single-photon ionization with a tunable vacuum-UV laser, fragmentation of organic compounds already sets in at a few electronvolts of excess energy provided by the laser photon. The important role of heating molecules by multiphoton absorption was discussed for fragmentation of similar organic compounds, and rates for internal conversion of the order of 10^{14} s^{-1} were reported.[54] In conclusion, nonresonant multiphoton ionization is unfavorable for reasonably large molecules (e.g., biomolecules) because of the large number of degrees of freedom that make the above-mentioned processes feasible. On the other hand, if femtosecond laser pulses are applied, the ionization rate may be able to compete with the conversion to internal energies. Care must be taken not to heat molecules excessively by providing excess energy, even with single-photon ionization. Future work will be dedicated to explore different ionization sources, such as the tunable vacuum-UV or femtosecond laser systems. Furthermore, less rigid molecules will be investigated.

In retrospect, thermionic emission and neutral fragmentation do not appear to be surprising; rather, they are the microscopic analogue of well-known macroscopic effects. Imagine heating a small piece of graphite in vacuum, e.g., by laser irradiation. As the object becomes heated to sufficient temperatures, evaporation of C, C_2, C_3, etc. will be observed (that is, neutral fragmentation in our microscopic terms). The object will also emit electrons like a filament (thermionic emission), and the small piece of graphite will glow and emit photons (blackbody emission). Moving toward finite particles (C_{60}), evaporative cooling and electron emission will be of increased and the blackbody emission will be of reduced importance.

Acknowledgment. We acknowledge stimulating discussions with Deborah H. Parker, Mike J. Pellin, and Dieter M. Gruen. This work was supported by the U.S. Department of Energy, BES-Materials Sciences, under Contract W-31-109-ENG-38.

References and Notes

(1) Rohlfing, E. A.; Cox, D. M.; Kaldor, A. *J. Chem. Phys.* **1984**, *81*, 3322–3330.
(2) Kroto, H. W.; Heath, J. R.; O'Brien, S. C.; Curl, R. F.; Smalley, R. E. *Nature* **1985**, *318*, 162–163.
(3) Krätschmer, W.; Lamb, L. D.; Fostiropoulos, K.; Huffman, D. R. *Nature* **1990**, *347*, 354–358.
(4) Curl, R. F.; Smalley, R. E. *Sci. Am.* **1991**, *Oct*, 54–63.
(5) Kroto, H. W.; Allaf, A. W.; Balm, S. P. *Chem. Rev.* **1991**, *91*, 1213–1235.
(6) Kroto, H. W.; McKay, K. *Nature* **1988**, *331*, 328–331.
(7) Wurz, P.; Lykke, K. R. *J. Chem. Phys.* **1991**, *95*, 7008–7010.
(8) Lykke, K. R.; Wurz, P. *J. Phys. Chem.* **1992**, 3191.
(9) Maruyama, S.; Lee, M. Y.; Haufler, R. E.; Chai, Y.; Smalley, R. E. *Z. Phys. D* **1991**, *19*, 409–412.
(10) Dietz, W.; Neusser, H. J.; Boesl, U.; Schlag, E. W. *Chem. Phys.* **1982**, *66*, 105–127.
(11) Boesl, U. *J. Phys. Chem.* **1991**, *95*, 2949–2962.
(12) Forst, W. *Theory of Unimolecular Reactions*; Academic Press: New York, 1973; Vol. 30.
(13) Klots, C. E. *Chem. Phys. Lett.* **1991**, *186*, 73–76.
(14) Hunt, J. E.; Lykke, K. R.; Pellin, M. J. In *Methods and Mechanisms for Producing Ions from Large Molecules*; Plenum Press: Minaki, Canada, 1991; pp 309–314.
(15) Parker, D. H.; Wurz, P.; Chatterjee, K.; Lykke, K. R.; Hunt, J. E.; Pellin, M. J.; Hemminger, J. C.; Gruen, D. M.; Stock, L. M. *J. Am. Chem. Soc.* **1991**, *113*, 7499–7503.
(16) Chatterjee, K.; Parker, D. H.; Wurz, P.; Lykke, K. L.; Gruen, D. M.; Stock, L. M. *J. Org. Chem.* **1992**, *57*, 3253–3254.
(17) Abrefah, J.; Olander, D. R.; Balooch, M.; Siekhaus, W. J. *Appl. Phys. Lett.* **1992**, *60*, 1313–1314.
(18) Pallix, J. B.; Schuehle, U.; Becker, C. H.; Huestis, D. L. *Anal. Chem.* **1989**, *61*, 805–811.
(19) Wurz, P.; Lykke, K. R.; Pellin, M. J.; Gruen, D. M.; Parker, D. H. *Vacuum* **1992**, *43*, 381–385.
(20) Wurz, P.; Lykke, K. R.; Pellin, M. J.; Gruen, D. M. *J. Appl. Phys.* **1991**, *70*, 6647–6652.
(21) O'Brien, S. C.; Heath, J. R.; Curl, R. F.; Smalley, R. E. *J. Chem. Phys.* **1988**, *88*, 220–230.
(22) Radi, P. P.; Bunn, T. L.; Kemper, P. R.; Molchan, M. E.; Bowers, M. T. *J. Chem. Phys.* **1988**, *88*, 2809–2814.
(23) Campbell, E. E. B.; Ulmer, G.; Hertel, I. V. *Phys. Rev. Lett.* **1991**, *67*, 1986–1988.
(24) Lichtenberger, D. L.; Jatcko, M. E.; Nebesny, K. W.; Ray, C. D.; Huffman, D. R.; Lamb, L. D. In *Mater. Research Society Symposia Proceedings*; Materials Research Society: Boston, 1991; Vol. 206, pp 673–678.
(25) Raghavachari, K.; Binkley, J. S. *J. Chem. Phys.* **1987**, *87*, 2191–2197.
(26) Amrein, A.; Simpson, R.; Hackett, P. *J. Chem. Phys.* **1991**, *94*, 4663–4664.
(27) Amrein, A.; Simpson, R.; Hackett, P. *J. Chem. Phys.* **1991**, *95*, 1781–1800.
(28) Cox, D. M.; Reichmann, K. C.; Kaldor, A. *J. Chem. Phys.* **1988**, *88*, 1588–1597.
(29) Leach, S.; Vervloet, M.; Despres, A.; Breheret, E.; Hare, J. P.; Dennis, T. J.; Kroto, H. W.; Taylor, R.; Walton, D. R. M. *Chem. Phys.* **1992**, *160*, 451–466.
(30) Lykke, K. R.; Wurz, P.; Parker, D. H.; Pellin, M. J. *Appl. Opt.*, in press.
(31) Pratt, S. T.; Dehmer, J. L.; Dehmer, P. M. *J. Chem. Phys.* **1985**, *82*, 676–680.
(32) Stanton, R. E.; Newton, M. D. *J. Phys. Chem.* **1988**, *92*, 2141–2145.
(33) Bethune, D. S.; Meijer, G.; Tang, W. C.; Rosen, H. J.; Golden, W. G.; Seki, H.; Brown, C. A.; deVries, M. S. *Chem. Phys. Lett.* **1991**, *179*, 181–186.
(34) Haarhoff, P. C. *Mol. Phys.* **1963**, *7*, 101–117.
(35) Spangenberg, K. R. *Vacuum Tubes*; McGraw-Hill: New York, 1948.
(36) Zimmerman, J. A.; Eyler, J. R.; Bach, S. B. H.; McElvany, S. W. *J. Chem. Phys.* **1991**, *94*, 3556–3562.
(37) Wang, L. S.; Conceicao, J.; Jin, C.; Smalley, R. E. *Chem. Phys. Lett.* **1991**, *182*, 5–11.
(38) Radi, P. P.; Hsu, M.; Rincon, M. E.; Kemper, P. R.; Bowers, M. T. *Chem. Phys. Lett.* **1990**, *174*, 223–228.
(39) Yoo, R. K.; Ruscic, B.; Berkowitz, J. *J. Chem. Phys.* **1992**, *96*, 911–918.
(40) Bagratashvili, V. N.; Dolzhikov, V. S.; Letokhov, V. S.; Makarov, A. A.; Ryabov, E. A.; Tyakht, V. V. *Sov. Phys. JETP* **1979**, *50*, 1075–1083.
(41) Christian, J. F.; Wan, Z.; Anderson, S. L. *J. Phys. Chem.* **1992**, submitted for publication.
(42) Beck, R. D.; John, P. S.; Alvarez, M. M.; F., D.; Whetten, R. L. *J. Phys. Chem.* **1991**, *95*, 8402–8409.
(43) Mowrey, R. C.; Brenner, D. W.; Dunlap, B. I.; Mintmire, J. W.; White, C. T. *J. Phys. Chem.* **1991**, *95*, 7138–7142.
(44) Stanton, R. E. *J. Phys. Chem.* **1992**, *96*, 111–118.
(45) Yi, J.-Y.; Bernholc, J. *J. Chem. Phys.* **1992**, *96*, 8634–8636.
(46) Sension, R. J.; Phillips, C. M.; Szarka, A. Z.; Romanow, W. J.;

McGhie, A. R.; McCauley, J. P.; Smith, A. B.; Hochstrasser, R. M. *J. Phys. Chem.* **1991**, *95*, 6075–6078.
(47) Letokhov, V. S. In *Laser spectroscopy of highly vibrationally excited molecules*; Letokhov, V. S., Ed.; Adam Hilger: New York, 1989; pp 1–54.
(48) Hare, J. P.; Kroto, H. W.; Taylor, R. *Chem. Phys. Lett.* **1991**, *177*, 394–398.
(49) Levine, R. D.; Bernstein, R. B. In *Molecular Reaction Dynamics and Chemical Reactivity*; Oxford University Press: Oxford, 1987; pp 117–206.
(50) Stone, A. J.; Wales, D. J. *Chem. Phys. Lett.* **1986**, *128*, 501–503.
(51) Gspann, J. *Z. Phys. D* **1986**, *3*, 143–145.
(52) Smalley, R. E. In *Atomic and Molecular Clusters*; Bernstein, E. R., Ed.; Elsevier: New York, 1990; pp 1–68.
(53) van Bramer, S. E.; Johnston, M. V. *Appl. Spectrosc.* **1992**, *46*, 255–261.
(54) Nakashima, N.; Yoshihara, K. *J. Phys. Chem.* **1989**, *93*, 7763–7771.

Vibrational Circular Dichroism Study of (2*S*,3*S*)-Dideuteriobutyrolactone. Synthesis, Normal Mode Analysis, and Comparison of Experimental and Calculated Spectra

Petr Malon,† Loretta J. Mickley, Kathleen M. Sluis, Cheok N. Tam, Timothy A. Keiderling,*

Department of Chemistry, University of Illinois at Chicago, Box 4348, Chicago, Illinois 60680

Sid Kamath, Jack Uang, and James S. Chickos

Department of Chemistry, University of Missouri—St. Louis, 8001 Natural Bridge Road, St. Louis, Missouri 63121 *(Received: March 30, 1992; In Final Form: September 8, 1992)*

The preparation, characterization, infrared absorption, and vibrational circular dichroism (VCD) spectra of the title compound are presented. From ab initio quantum mechanical energy minimization, geometry optimization calculations, the lowest energy conformation is a slightly distorted envelope form, so that deuteration give rise to both pseudoaxially and pseudoequatorially substituted conformers. The vibrational spectra (IR and Raman) have been assigned by comparison of frequencies and overall intensity patterns to those calculated by using an ab initio force field obtained for both conformers. This force field was subsequently modified by refining scale factors to improve the fit to frequencies of assigned bands for both the d_0 and d_2 isotopomers. The absorption intensities and VCD signs and magnitudes were calculated by the ab initio magnetic field perturbation theory of Stephens using the distributed origin gauge with origins at the nuclei. Good qualitative agreement was found between the experimental and theoretical dipole strengths and rotational strengths when the average of the calculated values for the two conformers was used. The best calculations used a 6-31G** basis set for for the force field and the intensities, but the refined force field did not lead to a significant improvement in the intensity or VCD pattern (other than frequency alignment) as compared to the unscaled ab initio result. For purposes of comparison to previous reports, calculations were also made for the planar conformation. Test calculations with variants of more approximate methods that do not allow for charge reorganization associated with nuclear motion gave distinctly unsatisfactory results, particularly in the mid-infrared portion of the spectrum.

Introduction

Vibrational circular dichroism (VCD), the measurement of the differential absorption of left and right circularly polarized light by molecular vibrational transitions, is a technique that has developed over the last 2 decades and has application for the study of the conformation of chiral molecules in solution.[1-6] It is clear from empirical studies that VCD has high sensitivity to change in molecular structure, but full utilization of VCD for stereochemical studies is dependent on development of a reliable relationship between structure and spectra. Ideally this structure–spectra relationship would involve calculation of spectra based on a well-founded theoretical understanding of the phenomenon being observed.

Existing theoretical models of VCD have met with varying nonsystematic success as well as failures. However, an apparently reliable method for calculating VCD intensities has been developed by Stephens and co-workers.[7-10] A similar theoretical formalism was proposed independently by Galwas, Fowler, and Buckingham[11] and these are sometimes referred to as the magnetic field perturbation (MFP) method. While shown to be successful in a number of cases where experiment and theory can be compared,[9,10] the ab initio MFP method has also been shown to be limited because of its apparent restriction to the use of fairly large basis sets for calculation of ab initio wave functions.[8] This proves to be impractical for many molecules of stereochemical interest.

We have undertaken a series of studies of the VCD spectra for small chiral molecules with a long-range goal of analyzing the differences between the predictions of this MFP method and those of simpler and very much more approximate methods and comparison of both types of predictions to real experimental data. If it should be possible to demonstrate that one of these simpler models is reliable, even on a qualitative basis for a limited subset of molecules or limited types of molecular vibrations, the broader applicability of such calculations to larger molecules of more general interest would justify the effort. To show such applicability, several analyses need to be done and a variety of molecules need to be studied. Such a broad theoretical and experimental study may, after analysis of the results, indicate which are the essential components needed in a theoretical model for a calculation of VCD that would be useful for structural interpretation. It should be clear that "usefulness" and exactness (or even accuracy) are not equivalent. For many molecules, the stereochemical questions of interest are quite restrictive; one often needs only to discriminate among a few possible conformations. At that level, VCD sign patterns or approximate intensities for a few key modes may be entirely sufficient.

With these overall goals in mind we have set out to prepare and study the IR and VCD spectra of a number of small-ring compounds made optically active by isotopic substitution. Such molecules are particularly appropriate for VCD study as they typically have significant VCD spectra,[12-16] and VCD can be used to monitor any structural changes that occur in them via chemical transformations.[13] On the other hand, these molecules often have very weak electronic CD spectra (normally measured in the UV)

*To whom correspondence should be addressed.
† Permanent address: Institute of Organic Chemistry and Biochemistry, Czechoslovak Academy of Sciences, Flemingovo nam. 2, Prague 6, CSFR.

0022-3654/92/2096-10139$03.00/0